A Detailed Performance Model for Bifacial PV Modules

Clifford Hansen[1], Daniel Riley[1], Chris Deline[2], Fatima Toor[3], Joshua Stein[1]

[1]Sandia National Laboratories, Albuquerque, NM, 87109 USA
[2]National Renewable Energy Laboratory, Golden, CO, USA
[3]The University of Iowa, Iowa City, IA, 52242, USA

***Abstract* — We present a detailed performance model for bifacial PV modules. Our model employs configuration factors to compute irradiance the rear surface of each cell in the module, estimates cell temperatures from irradiance and ambient temperature, and predicts of P_{MP}. Model performance is analyzed using measurements of bifacial module performance outdoors in Albuquerque, NM, USA.**

I. Introduction

Bifacial photovoltaic (PV) modules can accept light on both the front and rear surfaces. Currently, research efforts are underway to describe, test, rate, and model bifacial PV modules, as bifacial PV becomes a larger portion of the overall PV market. Sandia National Laboratories (Sandia), the National Renewable Energy Laboratory (NREL) and the University of Iowa are working together to provide the necessary data and analysis to better describe and predict bifacial PV performance to facilitate wider adoption throughout the PV market.

Our effort to develop a detailed performance models for bifacial PV modules seeks to create an accurate and computationally efficient model to predict the output of a bifacial PV system under any weather conditions and for a wide range of module orientations and system configurations, similar to the effort reported in [1]. Our effort is informed by extensive data describing measured performance of bifacial modules outdoors in a wide range of configurations [2]. Available performance models, e.g., [3], [4], typically estimate annual performance ratio or annual energy by means of correlations between module orientation and the *bifacial gain*, a ratio between power when both sides of the module receive illumination and power when only the front side is illuminated.

We test our model using data collected for bifacial modules mounted on a south-facing adjustable tilt rack (Fig. 1) with monofacial PV modules on the west half (left in figure) and bifacial PV modules on the east half. Reference cells measure irradiance along the middle of the rack: at the top and bottom of the front, and at the top, middle and bottom of the rear. Reference cells are calibrated outdoors against a primary reference cell (calibrated by NREL) to reduce variation among cells to less than 4 W/m^2 at irradiance of 1000 W/m^2.

II. Modeling Approach

The performance model for bifacial PV systems comprises a sequence of sub-models similar to the approach employed for modeling monofacial PV. Separation of irradiance into direct and diffuse components (if needed) is followed by translation to the module's plane using the same methods employed for monofacial modules. A configuration factor approach is used to estimate irradiance cell by cell on the module's back surface. Front and rear-side irradiance can be adjusted to account for reflection, shading, irradiance spectrum, and soiling. Cell temperature is estimated from irradiance and weather; cell temperature and irradiance are then used with calibrated cell models to estimate the IV curve for the module.

Fig. 1. Sandia's adjustable rack for measuring bifacial PV module performance.

A. Front and Rear Irradiance

The irradiance available for the front surface of bifacial PV modules is modeled in the same manner as for monofacial PV. Similar methods of transposing direct and diffuse irradiance onto a tilted surface may be used, and the site albedo can be used to estimate the amount of ground-reflected light present on the front surface.

Determining the irradiance on the rear side of a PV module requires new models. Rear side irradiance comprises primarily diffuse irradiance by way of reflections from the ground and other nearby surfaces, sky diffuse irradiance, with rare circumstances when direct irradiance illuminates the rear surface [5]. The module's orientation, proximity to nearby surfaces, and transparency [6] affect the area of ground and nearby surfaces and fraction of the sky visible from the module's rear surface. Rear-side irradiance models at different levels of detail are needed to support analyses from module and system design to annual energy production assessments [7].

Rear side irradiance can vary substantially depending on a module's position in the row, and rear irradiance may vary by more than 50 W/m^2 across a module's back surface [5]. A cell-level rear-side irradiance model [5] can estimate the irradiance mismatch across a single module and between modules in an array. An array-scale model [8] computes irradiance along a cross-section of a fixed-tilt array with

regular rows; the computational simplicity makes this model suitable for energy production assessments for large systems. A similar approach can be used to model rear-surface irradiance for bifacial modules on horizontal east-west single axis trackers [9]. Ray-tracing models (e.g., [10]) provide detailed assessment of effects of module design details, such as cell to cell spacing and surface reflections, but with significant computational cost. Selecting the best method for determining rear irradiance may depend on the use case and requirements for computation time, accuracy, and resolution.

The detailed cell-level and the array-scale rear-surface irradiance models use view factors, also termed shape and view factors, configuration factors quantify the fraction of irradiance reflected from one surface that arrives at a receiving surface. View factor models [11], [3] calculate back surface irradiance E_2 (W/m^2) by

$$E_2 = \alpha \times G_1 \times F_{1\to 2} \qquad (1)$$

where G_1 is the total irradiance (W/m^2) on the reflecting area being considered (e.g., an area of the ground), α is the reflecting surface's albedo (unitless) and $F_{1\to 2}$ is the view factor (unitless) from the reflecting area to the receiving surface. The total irradiance on the back surface of a cell or module is the sum over all contributing surfaces. A view factor model implicitly assumes that all reflecting surfaces are Lambertian, i.e., irradiance is scattered isotropically.

Formally, view factors are calculated by integration (Eq. 2) using terms in the illustration. An emitting surface (dA1) reflects incident irradiance, part of which is incident on the receiving surface: the view factor $VF_{1\to 2}$ quantifies the fraction of irradiance emitted by dA1 that is received by dA2.

$$F_{1\to 2} = \frac{1}{A_1}\int_{A_1}\int_{A_2} \frac{\cos\theta_1 \cos\theta_2}{\pi s^2}\, \mathrm{d}A_2\, \mathrm{d}A_1 \qquad (2)$$

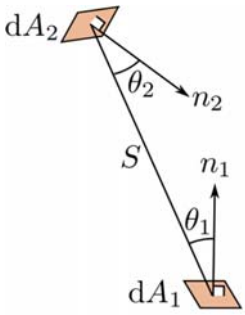

A rear surface irradiance model is assembled by specifying the set of reflecting surfaces and the irradiance incident on each surface. For example, irradiance on the sunlit ground is modeled by global horizontal irradiance (GHI) and irradiance on a shadowed area is modeled by diffuse horizontal irradiance (DHI), where each irradiance is reduced by the fraction of the hemispherical sky dome occluded by adjacent rows of modules.

Fig. 2 illustrates the modeled variation in rear-surface irradiance between cells at the edge of a row in the array (left side in figure) and cells toward the middle of a row (right side of figure). Cells at the left edge of the row receive significantly more rear-surface irradiance than cells in the middle of the row's modules, because edge cells 'see' sunlit ground to the left of the row. Cells at the lower and upper edges also receive more irradiance than middle cells because of sunlit areas in front of and behind the row's shadow. Sandia has developed an efficient method [5] for computing the required view factors; implemented in Matlab™; simulations with 150 time steps, 4 60-cell modules, and 10 nearby objects contributing shadows (modeling the adjustable rack shown in Fig. 1) were complete in about 15 seconds.

Calculation of view factors at a cell level permits modeling of rear-surface irradiance for arrays with subsets of modules in different configurations, e.g., a mix of southward facing, fixed tilt modules and vertical E-W facing modules. In concept, a cell-level irradiance model enables an array performance model to directly account for mismatch conditions among cells and modules, although explicit mismatch modeling is not done in our present work.

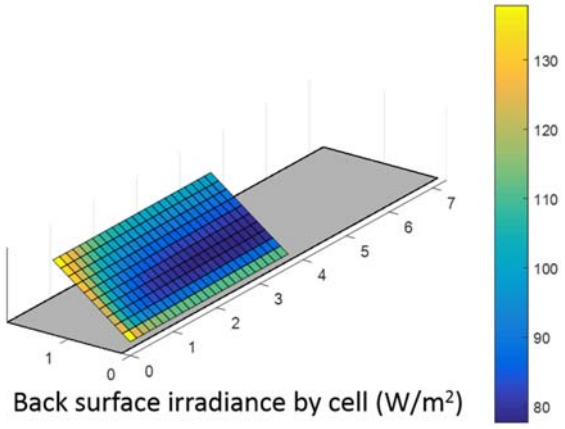

Fig. 2. Example calculation of cell-by-cell rear-surface irradiance, solar noon, assumed clear sky, single row of 8 modules in portrait orientation at fixed 35º tilt (left-most 4 modules shown).

B. Reflection, Shading, Spectrum and Soiling

Reflections. Reflections from a module's front surface are modeled as is done for monofacial modules (e.g., [12]): an empirically determined expression computes the fraction of the direct irradiance on the module's face is reflected away from the angle of incidence of the direct irradiance. Reflections from the rear surface are not explicitly represented; the effect of any reflections can accounted for in the empirical relationship between total incident irradiance (front surface + back surface) and the current produced by the module.

Shading. PV racking, junction boxes, or module wiring may shade parts of the rear-side of a bifacial PV module from irradiance sources. To discover the effects of rear-surface shading, we measured IV curves after placing cardboard strips in various locations and orientations behind a bifacial module (e.g., Fig 3, see [13] for experimental details). Comparison of IV curves with and without the obstructions showed that P_{MP} is generally reduced in proportion to the obstruction area, with the proportionality decreasing with increasing distance between the obstruction and the module. However, obstructions affected both I_{SC} and I_{MP} in a complicated manner depending on obstruction orientation; this is not surprising as obstructions across several cell strings

will have a different effect on current than obstructions confined to a single cell string (e.g., compare Fig. 3 and 4).

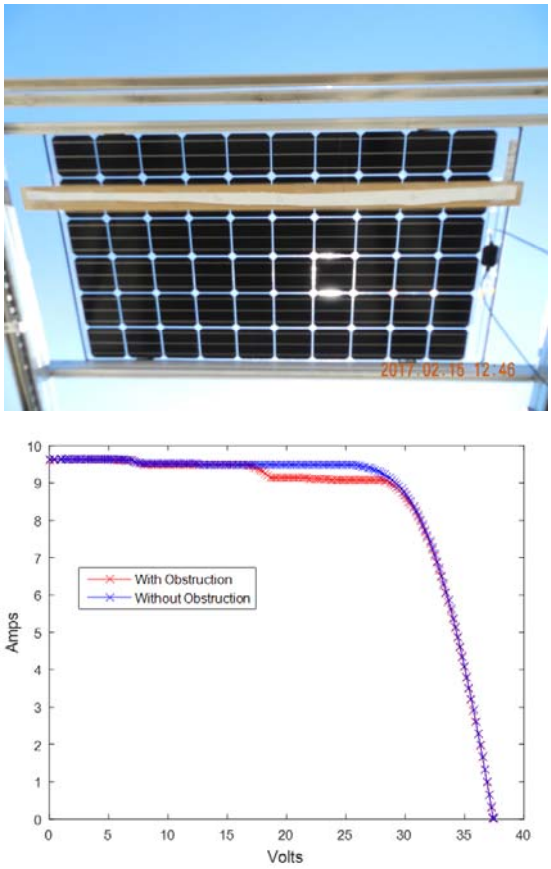

Fig. 3. Example of rear-surface irradiance obstruction experiment: obstruction (top) and measured IV curves (bottom).

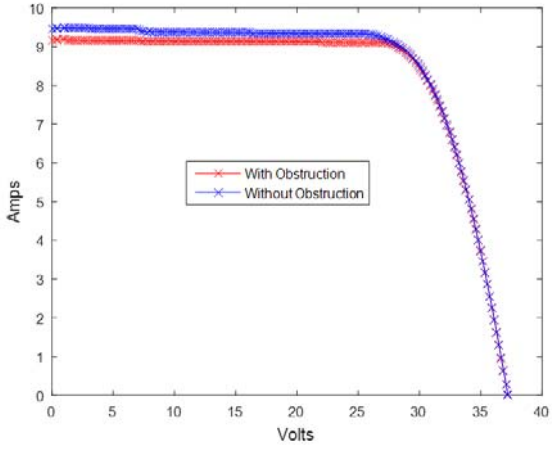

Fig. 4. IV curve with obstruction across cell strings rather than along a single string, as in Fig. 3.

The reduction of rear-surface irradiance due to obstructions can be modeled directly using ray-tracing methods. View factor methods appear suitable only for the simplest obstruction cases, e.g., a single rectangular obstruction with edges parallel to the module's edges. In either case, the computational effort to configure and complete the calculations appears impractical for power and energy simulations. As an alternative we propose the following simple model for the effect of obstructions on module P_{MP}:

$$P_{MPo} = P_{MP}\left(1 - k_{obs} \times A_{obs} / A_{\mathrm{mod}}\right) \qquad (3)$$

where P_{MPo} is the P_{MP} reduced by the effect of obstructions, A_{obs} and A_{mod} are the obstruction and module aperture areas, respectively, and k_{obs} is an empirical factor representing the effect of the distance between the obstructing objects and the module's rear surface. Module IV curves with obstructions (e.g. [13], Fig. 3) indicate values of k_{obs}=1.0 for obstructions placed against the module's rear surface, and k_{obs}=0.6 for obstructions placed ~5cm from the rear surface.

Spectrum. The spectrum of the incident light alters the module's current due to the spectral response of the module's cells. The effect of spectrum changes can be estimated with existing models, e.g., [14], [15]. Spectral irradiance on the rear side differs from spectral irradiance on the front side due to reflections from the ground and/or nearby objects. Here, we neglect the effect of spectrum of rear-surface irradiance, reasoning that its effect is less than the uncertainty in estimating the broadband rear-surface irradiance.

Soiling. We assume that the effects of soiling on bifacial PV modules can be represented by two factors applied to front and rear-surface irradiance, respectively. For bifacial modules at fixed tilts, we have observed little to no soil accumulation on the rear surfaces in Albuquerque, NM, USA. It stands to reason that vertical modules will accumulate soil equally on both faces, although we have no measurements available to quantify the accumulation of soil on vertical module surfaces.

C. Cell Temperature

Cell temperature can be modeled using an approach similar to that used for monofacial modules, e.g., [14]. We measured temperature with thermocouples attached in between cells on a bifacial module's rear-surface concurrent with ambient temperature and wind speed (at 3m above ground). The measurements verify that module temperature models in common use for monofacial modules also describe well the measured data for bifacial modules. For example, the module temperature model in [14]

$$T_{mod} = \left(E_f + E_r\right) \times \left[e^{a+b \cdot WS}\right] + T_{amb} \qquad (4)$$

fits well to the collected data: T_{mod} is the average temperature across the rear surface of the module, T_{amb} and WS are the ambient air temperature and wind speed (m/s), respectively, E_f and E_r are the front and rear surface irradiance (W/m^2) respectively, and a and b are empirical constants determined from the fitting. For glass-cell-glass modules in open racking, values of a = –3.47 and b = –0.0594 are suggested [14]. Cell temperature T_C is obtained from Eq. 4 as

$$T_C = T_M + \Delta T\left(E_f + E_r\right) / 1000 \qquad (5)$$

where ΔT = 3 ºC for open racking. We expect that other cell temperature models, e.g., [16] would be successful as well.

Fig. 5 shows the residuals when modeling a bifacial PV module temperature with Eq. 4. The blob of residual values lying below the linear tread generally corresponds with dynamic temperature conditions resulting from passing cloud shadows. Shading immediately reduces the irradiance and hence module temperature predicted by Eq. 4. In reality, module temperature decreases take place over time periods on the order of 10 minutes, thus, the steady-state model in Eq. 4 underpredicts module temperature after the transition from fully lit to shaded conditions. Similarly, module temperature is overpredicted after the transition from shaded to fully lit conditions.

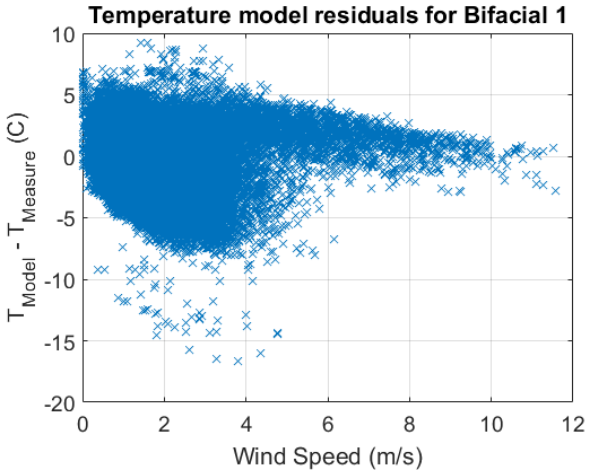

Fig. 5. Residuals for the module temperature model as a function of wind speed for a bifacial system.

Plots of the residuals for a co-located monofacial system exhibit nearly identical features and magnitudes: the RMSE of the model for the bifacial system is about 3.4 °C, while the RMSE for a co-located monofacial system is 3.1 °C. The similarities in model performance between bifacial and monofacial modules, and the physical reasoning behind Eq. 4 (see [14]), provide confidence that typical values for a and b determined for glass-glass monofacial modules should also be reasonable for bifacial modules.

D. Electrical Performance

We present a simple model for P_{MP} for bifacial PV modules akin to PVWatts [17] which can account for rear-surface shading by obstructions using Eq. 3. The model operates on cell average irradiance (front and rear surface); thus the effects of mismatch from cell-to-cell variation in irradiance are not explicit.

We estimate maximum power for a bifacial module, P_{MP} (W) from broadband front irradiance E_f (W/m^2), rear irradiance E_r (W/m^2), cell temperature T_C (ºC), module bifacial ratio R_b (unitless), temperature coefficient for maximum power γ (1/ºC) and the module power rating at STC conditions P_{MP0} (W).

$$P_{MP} = P_{MP0}\left(1+\gamma\left(T_C - T_0\right)\right) \times\left(M \times E_f + R_b \times E_r\right)/E_0 \times\left(1 - k_{obs} \times A_{obs}/A_{\text{mod}}\right) \quad (6)$$

The bifacial ratio R_b is the ratio of power produced by the rear side to the front side under identical illumination and temperature and P_{MP0} is determined by a front-side-only flash test at standard test conditions; these measurements are discussed in [6]. The term M in Eq. 6 represents the combined adjustment to front irradiance from spectrum, reflections and soiling.

III. Verification and Analysis

Fig. 6 compares the measured and modeled (using Eq. 6) maximum power for the top bifacial PV module on the adjustable rack, shown in Fig. 7. For the results in Fig. 6, the front irradiance E_f is the irradiance measured by a coplanar reference cell, and the rear irradiance E_r is estimated by averaging measurements from two reference cells adjacent to the module's western corners (indicated by green triangles in Fig. 7). For the test module P_{MP0} = 270 W and R_b = 0.93 as determined using IV curves measured separately for the front and rear. We set M = 1 because the reference cells have similar reflection and spectral response as the module under test. The mounting rack and connector wiring do not obstruct rear irradiance, thus A_o = 0. Except at high P_{MP}, the simple model predicts the module power to within 5W (about 2%), but at high P_{MP} the model overestimates power by as much as 20W (about 8%). The few points far below the 1:1 line likely result from temporary shadows affecting the front irradiance measurement, or bad data.

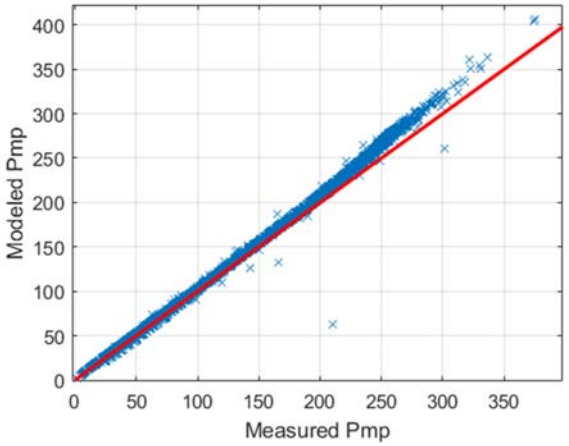

Fig. 6. Modeled and measured maximum power for a single bifacial PV module on 5-min intervals from 30 June to 25 July, 2016, in Albuquerque, NM. 1:1 line in red.

The overestimation at high P_{MP} could result from a combination of two causes:

1. Mismatch loss due to variation in rear-surface irradiance among cells.
2. Non-linear dependence of P_{MP} on irradiance and/or temperature.

The shadows on the ground cause variation among the rear-facing reference cells of up to 40 W/m^2 (top and middle cells indicated in Fig. 8). Similar variation is also present among the module's cells, so it is reasonable to anticipate a mismatch in current on the order of 3% (40W being roughly 3% of the total front+rear irradiance of around 1250 W/m^2), with a corresponding reduction in the module power. The mismatch would be most prominent during clear skies periods at midday, when irradiance is high and shadows on the ground are well-defined (see Fig. 7). In addition, the departure from linear dependence of power on irradiance may be a property of the particular bifacial module under test, a possibility we intend to investigate further.

Fig. 7. Bifacial PV module under test circled in red. Top and middle rear-facing reference cells indicated by green triangles. View is to the south.

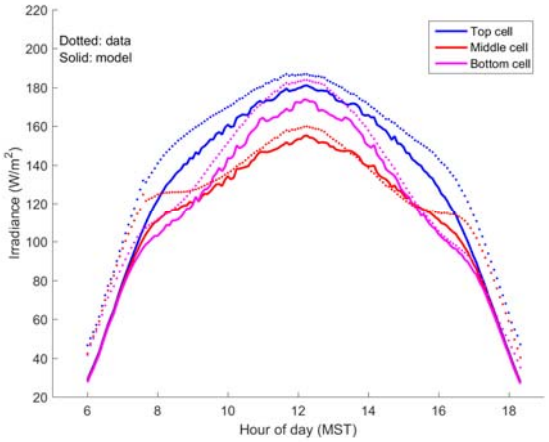

Fig. 8. Modeled and measured irradiance for rear-facing reference cells in the adjustable array: 14 July 2016, a clear day, array titled at 15º with center at 1.63m above ground.

With the above model discrepancies in mind, we compute P_{MP} using modeled rear-surface irradiance instead of the reference cell measurements. We use the cell-level rear-surface irradiance model described above (and detailed in [18]) to compute the cell-by-cell irradiance for the top-right bifacial module (6 × 10 cells in landscape orientation; Fig. 7). This model was previously verified [5] to be within 10% of measurements over a wide range of conditions using an array of rear-facing reference cells mounted on a module-sized plate (Fig. 11). Fig. 8 compares rear-surface irradiance model predictions with measurements for each of the three rear-facing reference cells. The model generally follows the trends in the data, although with a consistent underestimate of the measured values. Cell-by-cell modeling of the module (Fig. 9) shows a cell-to-cell variation as great as 50 W/m^2, or roughly 5% of total (front + back) irradiance of 1250 W/m^2 at midday.

Fig. 10 compares residuals for predicted P_{MP} using either measured or modeled rear-surface irradiance. The model overestimates P_{MP} by approximately 20 W (about 7%) at full sun conditions, with either irradiance source. Causes for the overestimate include mismatch losses not accounted for by the model, or module behavior, as previously discussed. Two bands are apparent in the residuals when using measured rear-surface irradiance at moderate P_{MP} levels. These bands result from the dynamic effect on ground-reflected irradiance of the passage of the sunlit and shadowed areas beneath the cell as the sun moves from east to west. The bands are not present when using the modeled rear-surface irradiance because of the module's larger aperture smooths these dynamics to a large extent.

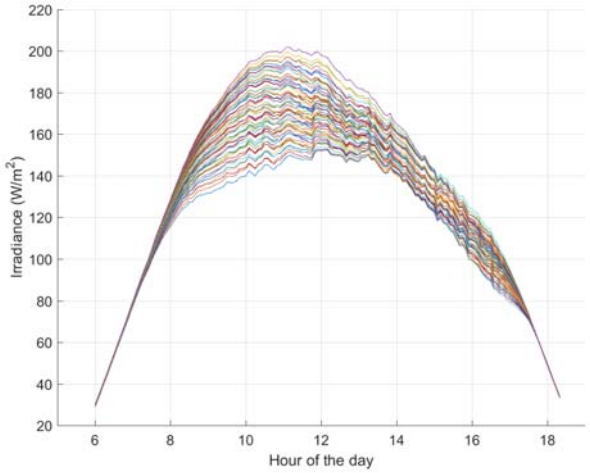

Fig. 9. Modeled rear irradiance by cell on the top right bifacial module in the adjustable array: 6 July 2016, a clear day, array titled at 15º with center at 1.63m above ground.

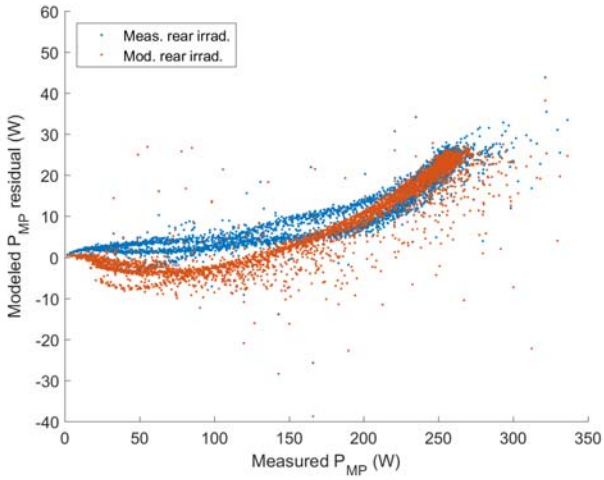

Fig. 10. Residual of modeled PMP using modeled and measured rear irradiance.

Fig. 11. Sandia's high spatial resolution rear irradiance module blank with ten reference cells measuring rear irradiance, used for validation of the irradiance model.

ACKNOWLEDGEMENTS

Sandia National Laboratories is a multi-mission laboratory managed and operated by National Technology & Engineering Solutions of Sandia, LLC., a wholly owned subsidiary of Honeywell International, Inc., for the U.S. Department of Energy's National Nuclear Security Administration under contract DE-NA0003525.

REFERENCES

1. Janssen, G.J.M., et al., *Outdoor Performance of Bifacial Modules by Measurements and Modelling.* Energy Procedia, 2015. **77**: p. 364-373.
2. Stein, J., C. Deline, and F. Toor, *Outdoor Field Performance from Bifacial Photovoltaic Modules and Systems*, in *44th IEEE Photovoltaic Specialist Conference*. 2017: Washington, DC.
3. Yusufoglu, U.A., et al., *Simulation of Energy Production by Bifacial Modules with Revision of Ground Reflection.* Energy Procedia, 2014. **55**: p. 389-395.
4. Wang, S., et al., *Bifacial Photovoltaic Systems Energy Yield Modelling.* Energy Procedia, 2015. **77**: p. 428-433.
5. Hansen, C.W., et al., *A Detailed Model of Rear-Side Irradiance for Bifacial PV Modules*, in *44th IEEE Photovoltaic Specialist Conference*. 2017: Washington, D.C., USA.
6. Deline, C., et al., *Evaluation and Field Assessment of Bifacial Photovoltaic Module Power Rating Methodologies*, in *43rd IEEE Photovoltaic Specialist Conference*. 2016: Portland, OR.
7. Hansen, C.W., et al., *Analyis of Irradiance Models for Bifacial PV Modules*, in *43rd IEEE Photovoltaic Specialist Conference*. 2016: Portland, OR.
8. Marion, B., et al., *A Practical Irradiance Model for Bifacial PV Modules*, in *44th IEEE Photovoltaic Specialist Conference*. 2017: Washington, DC.
9. Anoma, M., et al., *View Factor Model and Validation for Bifacial PV and Diffuse Shade on Single-Axis Trackers*, in *44th IEEE Photovoltaic Specialist Conference*. 2017: Washington D.C., USA.
10. Asgharzadeh, A., et al., *Analysis of the Impact of Installation Parameters and System Size on Bifacial Gain and Energy Yield of PV Systems*, in *44th IEEE Photovoltaic Specialist Conference*. 2017: Washington, DC.
11. Iqbal, M., *An Introduction to Solar Radiation*. 1983, Toronto: Academic Press Canada.
12. Martin, N. and J.M. Ruiz, *Calculation of the PV modules angular losses under field conditions by means of an analytical model.* Solar Energy, 2001. **70**: p. 25-38.
13. Riley, D., et al., *A Performance Model for Bifacial PV Modules*, in *44th IEEE Photovoltaic Specialist Conference*. 2017: Washington, DC.
14. King, D.L., E.E. Boyson, and J.A. Kratochvil, *Photovoltaic Array Performance Model*. 2004, Sandia National Laboratories: Albuquerque, NM.
15. Lee, M. and A. Panchula, *Combined Air Mass and Precipitable Water Spectral Correction for PV Modelling*, in *4th PV Performance Modeling and Monitoring Workshop*. 2015: Cologne, Germany.
16. Faiman, D., *Assessing the outdoor operating temperature of photovoltaic modules.* Progress in Photovoltaics: Research and Applications, 2008. **16**(4): p. 307-315.
17. Dobos, A., *PVWatts Version 5 Manual*. 2014, National Renewable Energy Laboratory.
18. Hansen, C.W. and D. Riley, *A Computationally Efficient Method for Detailed Modeling of Rear-Side Irradiance for Bifacial PV Modules*, in *44th IEEE Photovoltaic Specialist Conference*. 2017, IEEE: Washington, D.C., USA.